Journal of Physics D: Applied Physics

PAPER • OPEN ACCESS

Operating principles of zero-bias retinomorphic sensors

To cite this article: John G Labram 2023 *J. Phys. D: Appl. Phys.* **56** 065105

View the article online for updates and enhancements.

You may also like

- An Energy-Efficient Routing Protocol for ZigBee Networks
Qijin Wang, Dandan Wang and Xiaoxia Qi
- Efficient coupling of self-collimated beams to slow light modes of a coupled zigzag-box resonator via antireflection structures in a photonic crystal
Sun-Goo Lee and Chul-Sik Kee
- Quantifying the performance of perovskite retinomorphic sensors
Cinthya Trujillo Herrera and John G Labram

ECS Toyota Young Investigator Fellowship

ECS TOYOTA

For young professionals and scholars pursuing research in batteries, fuel cells and hydrogen, and future sustainable technologies.

At least one $50,000 fellowship is available annually.
More than $1.4 million awarded since 2015!

Application deadline: January 31, 2023

This content was downloaded from IP address 128.41.35.204 on 23/01/2023 at 16:58

IOP Publishing

Journal of Physics D: Applied Physics

J. Phys. D: Appl. Phys. **56** (2023) 065105 (13pp) https://doi.org/10.1088/1361-6463/acb0de

Operating principles of zero-bias retinomorphic sensors

John G Labram

Department of Electronic & Electrical Engineering, University College London, London WC1E 7JE, United Kingdom

School of Electrical Engineering and Computer Science, Oregon State University, Corvallis, OR 97331, United States of America

E-mail: j.labram@ucl.ac.uk

Received 19 August 2022, revised 20 December 2022

Accepted for publication 6 January 2023

Published 23 January 2023

Abstract

Zero bias retinomorphic sensors (ZBRSs) are a new type of optical sensor which produce a signal in response to changes in light intensity, but not to constant illumination. For this reason, they are hoped to enable much faster identification of moving objects than conventional sensing strategies. While recent proof-of-principle demonstrations are significant, there does not yet exist a robust quantitative model for their behaviour, which represents an impediment for effective progress to be made in this field. Here I report a mathematical framework to quantify and predict the behaviour of ZBRSs. A simple device-level model and a more detailed carrier-dynamics model are derived. Both models are tested computationally, yielding equivalent behaviour consistent with experimental observations. A figure of merit, Λ_0, was identified which is hoped to enable facile comparison of devices between different research groups. This work is hoped to serve as the foundation for a consistent description of ZBRSs.

Supplementary material for this article is available online

Keywords: sensors, retinomorphic thin film sensor, organic semiconductors, retinomorphic, retinomorphic sensor

(Some figures may appear in colour only in the online journal)

1. Introduction

A retinomorphic thin film sensor (RTFS) is a biologically-inspired [1, 2] optical sensor designed to respond to changes in light intensity, rather than to light intensity itself [3]. By producing a non-zero signal only when movement occurs, these sensors are hoped to enable rapid identification of moving objects. Unlike conventional event-driven optical sensors [4, 5], which employ silicon-based differential amplifiers [6, 7], RTFSs are formed of just a thin-film photosensitive bilayer capacitor (see figure 1(a)) and a resistor in series [3]. For this reason, it is hoped that they could one day offer a more simple sensing paradigm, and ultimately higher density, lower cost, and faster response, than other event-driven sensors.

RTFSs are a new technology and are poorly understood. Our first devices employed a metal halide perovskite (commonly abbreviated to just 'perovskite') [8] as an absorber layer, and required a non-zero applied input voltage, V_{in}, to produce a significant response (see figure 1(b)) [3]. We have more recently demonstrated devices, employing an organic semiconductor blend [9], which operate with no input connection and just an output (see figure 1(c)) [10]. These results have proven our previous device model to be incomplete, as it was not able to describe the generation of an output

Original content from this work may be used under the terms of the Creative Commons Attribution 4.0 licence. Any further distribution of this work must maintain attribution to the author(s) and the title of the work, journal citation and DOI.

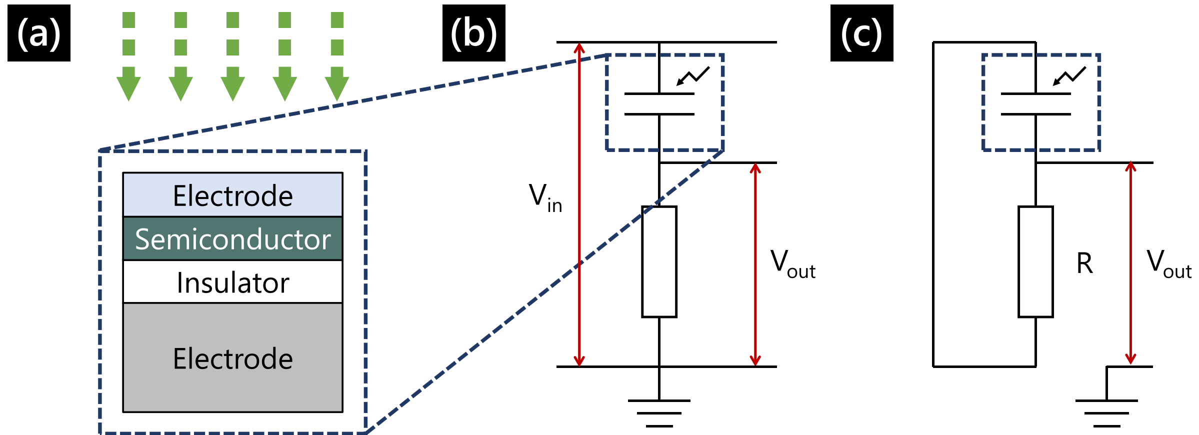

Figure 1. (a) Cross sectional schematic diagram of photosensitive capacitor used in retinomorphic thin film sensor (RTFS). (b) Circuit diagram of RTFS sensor consisting of photosensitive capacitor (top) and resistor (bottom). (c) Circuit diagram of zero-bias retinomorphic sensor (ZBRS).

voltage without a finite input voltage [11]. Sensors based on this, or a similar, design have also previously been referred to as photocells [12, 13], transient photodetectors [14], and differential photodetectors [15]. The purpose of this report is to provide a robust, quantitative, and phenomenological description of RTFSs operating with no applied bias. In the interest of brevity, I shall henceforth refer to a retinomorphic sensor that operates with zero input voltage as a zero-bias retinomorphic sensor (ZBRS).

2. Experimental details

2.1. RTFS fabrication and characterisation

All experimental devices measured in this report were fabricated as part of our previous work [10], and were re-measured after approximately 2 months storage at room temperature, in the dark, in inert atmosphere N_2. The photosensitive capacitors consist of four layers (see figure 1(a)) which are from bottom to top: an electrode, an insulator, a photo-active semiconductor, and another electrode. In this case these layers were highly doped silicon, 300 nm thermally grown silicon dioxide (SiO_2), a 1:1 (weight %) blend of poly(3-hexylthiophene-2,5-diyl) (P3HT) with phenyl-C_{61}-butyric acid methyl ester (PCBM), and 100 nm indium tin oxide (ITO), respectively.

2.2. RTFS characterisation

All devices were contacted in an ambient-pressure N_2 glovebox at room temperature using an Everbeing C-2 probe station. The devices were connected in series with a conventional resistor (100 kΩ in all cases studied experimentally), which was held outside of the glovebox. The voltage dropped across the external resistor (V_{out}) was monitored with a Textronix TBS2072B digital oscilloscope. Illumination was provided with a ThorLabs SOLIS-525C High-Power Green (525 nm) light emitting diode (LED), controlled with a ThorLabs DC2200 LED Controller.

3. Experimental results

A square wave of green (535 nm) light with an optical power density minimum of $P = 0$ mW cm^{-2} and a maximum between $P = 0.35$ mW cm^{-2} and 124 mW cm^{-2} was applied to the photosensitive capacitor, with a frequency of 100 Hz. The intended form of this optical power density is depicted in figure 2(a). The top electrode was grounded (i.e. $V_{in} = 0$ V) and the output voltage across the resistor, V_{out}, was measured as a function of time. An example is shown for a 100 kΩ resistor and a maximum optical power density of 23.6 mW cm^{-2} in figure 2(b). The device behaves as expected: producing a spike in V_{out} in response to the light being turned on or off, but otherwise outputting $V_{out} = 0$ V. The device again exhibits the characteristic features from our original report [10]: a negative V_{out} in response to the light turning on, a positive V_{out} in response to the light turning off, and a spike with a larger magnitude in response to the light being turned off. The peak voltage, defined as V_{max}, was extracted for the light turning on and turning off, as a function of the peak P in the square wave. This data is plotted in figure 2(c).

4. Simple device model

In our original experimental demonstration of ZBRSs, we hypothesised that an imbalance of holes and electrons in the semiconductor under quasi-steady state illumination conditions could explain our observation of a non-zero V_{out} spike when $V_{in} = 0$ [10]. However, we have since observed that the device will output a signal without a ground connection at all (i.e. when configured as in figure 1(c)) [16]. This means our previous description was incomplete.

I here propose two strategies to quantify the voltage-time behaviour of ZBRSs. The first is based on circuit-level parameters only, and the second also on carrier generation, recombination, and diffusion in the absorber. Central to both strategies is the assertion that the charge on each plate of the photo-sensitive capacitor need not necessarily be equal and

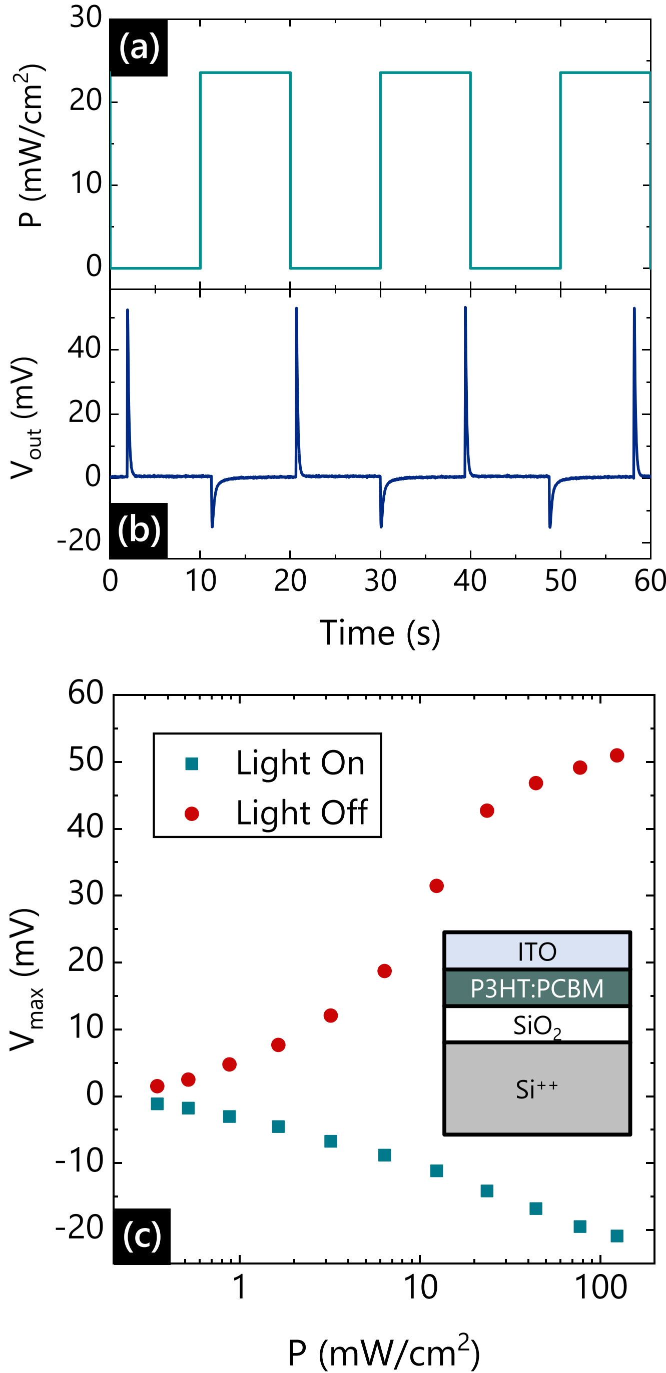

Figure 2. (a) Expected optical power density (P) as a function of time incident on photosensitive capacitor used in example ZBRS. (b) Experimentally measured output voltage (V_{out}) as a function of time in response to square wave optical power density. (c) Peak value of voltage spike, V_{max}, in response to square wave illumination from 0 to P, extracted from experimental data of V_{out} vs t, in response to light turning on (green) and light turning off (red). Inset: cross sectional diagram of photosensitive capacitor used in ZBRS (not to scale).

opposite at all times. In the simple device model, I will make the approximation that charge generation and recombination both occur instantly, which is a reasonable approximation when the RC time constant of the ZBRS is $>>1$ μs, but may not encapsulate all relevant phenomena. The second model considers the dynamics of holes and electrons in the absorber, enabling more insight, but may not be practical for routine or high-throughput device characterisation.

In both cases, it is assumed that the top electrode will allow only one type of carrier to exit the device. i.e. electrons or holes are able to cross the metal/semiconductor interface but not both. For conciseness, I will henceforth describe only the situation where holes can exit and electrons cannot, but the theory is general. This description is anticipated to be appropriate for the device depicted in the inset of figure 2(c), as the highest occupied molecular orbital of a P3HT:PCBM blend is well aligned with the work function of ITO [17], but the lowest unoccupied molecular orbital of P3HT:PCBM is not well aligned with the work function of ITO.

I begin by considering each plate of our photosensitive capacitor separately. I define the bottom plate as the bottom metallic electrode (Si^{++} in the inset to figure 2(c)), and the net charge on this plate as Q_{B}. The top plate is defined as the semiconductor absorber (P3HT:PCBM in the inset to figure 2(c)), and the net charge on this plate is Q_{T}. Throughout this description, the capacitor and resistor are in parallel, with V_{out} defined at the connection between the bottom electrode of the capacitor and the resistor. This description is depicted diagrammatically in figure 3 for the example of a step change in illumination intensity, but the theory is valid for incident light with any time-dependence. In this example, a light is turned on and left on at $t = t_0$. The approximation is made that under constant illumination electrons and holes are generated instantly in roughly equal number [18]. Because only holes can cross the metal/semiconductor interface, diffusion will cause some holes, but no electrons, to leave the semiconductor at $t = t_1$, and a net negative charge will accumulate in the semiconductor. For subsequent times $t_2 \geqslant t > t_3$ a positive charge flows from the top electrode, through the resistor, onto the bottom plate to balance the charge on the top plate. For long time scales, denoted t_3 here, the system will be in equilibrium, no more current will flow, and $Q_{\mathrm{B}} = -Q_{\mathrm{T}}$.

To quantify this behaviour, I start with an equation for the rate of change of net charge density on the top electrode, $\dot{Q}_{\mathrm{T}}$. This will have contributions from two terms: one for the change in charge density due to illumination ($\dot{Q}_{\mathrm{T}}|_{\mathrm{light}}$), and one due to charge flow in the circuit ($\dot{Q}_{\mathrm{T}}|_{\mathrm{flow}}$):

$$\frac{\mathrm{d}Q_{\mathrm{T}}}{\mathrm{d}t} = \left.\frac{\mathrm{d}Q_{\mathrm{T}}}{\mathrm{d}t}\right|_{\mathrm{light}} + \left.\frac{\mathrm{d}Q_{\mathrm{T}}}{\mathrm{d}t}\right|_{\mathrm{flow}}. \tag{1}$$

I start by evaluating the change in charge due to current flow (i.e. $\dot{Q}_{\mathrm{T}}|_{\mathrm{flow}}$). With the assertion that in general $Q_{\mathrm{B}}(t) \neq -Q_{\mathrm{T}}(t)$, the field resulting from each plate must be defined separately. Solving Gauss' Law for an infinite flat plate [19], the electric field due to the charge on the top plate, E_{T}, is defined as:

$$E_{\mathrm{T}} = \frac{\sigma_{\mathrm{T}}}{2\varepsilon_r\varepsilon_0} \tag{2}$$

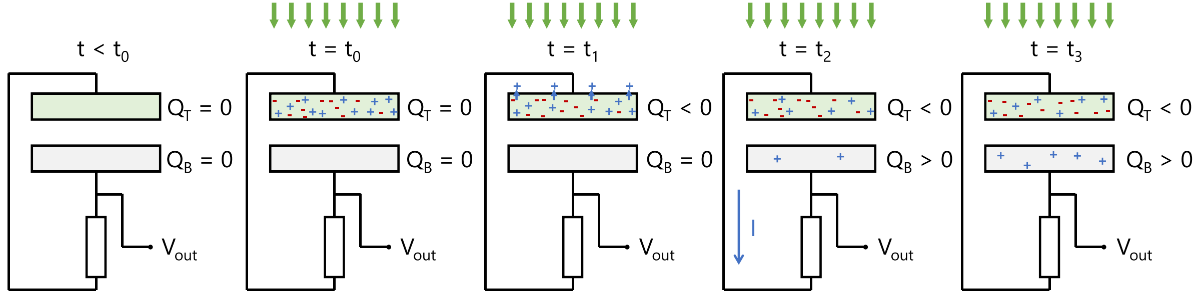

Figure 3. Diagrammatic representation of operating mechanism of ZBRS employed in the simple device model. The green top region depicts the semiconductor, the white region the impassable insulator, and the light grey region the bottom metallic electrode. The blue '+' symbols denote free holes and the red '−' symbols denote free electrons. The light is turned on and left on at time $t = t_0$ with a constant light intensity.

Here, σ_T is the two dimensional (2D) charge density (units of e.g. C cm^{-2}) on the top plate, ε_r is the relative permittivity of the medium between the plates, and ε_0 is the vacuum permittivity. The approximation of an infinite plane neglects edge effects, which is valid when the plate separation is small relative to the plate area. Because our experimental plate area is ∼1 mm^2 and the plate separations is ∼100 nm, I take this approximation as true for the devices studied here. However this approximation could be invalidated if pixel dimensions become comparable to dielectric thickness, or if the device experiences extreme curvature [20]. The potential at the bottom plate, V_B, resulting from this field on the top plate is therefore:

$$V_\mathrm{B} = -\frac{\sigma_\mathrm{T} d}{2\varepsilon_r \varepsilon_0}. \tag{3}$$

Here d is the separation of the plates. Note I use the notation V_B because this is the potential at the bottom plate, even if it is resulting from charge on the top plate. This is the voltage relative to ground. Expressing this in terms of total charge on the top plate, $Q_\mathrm{T} = A\sigma_\mathrm{T}$, where A is the plate area:

$$V_\mathrm{B} = -\frac{Q_\mathrm{T} d}{2\varepsilon_r \varepsilon_0 A}. \tag{4}$$

Identifying the capacitance of the parallel plate capacitor as $C = \varepsilon_r \varepsilon_0 A/d$:

$$V_\mathrm{B} = -\frac{Q_\mathrm{T}}{2C}. \tag{5}$$

Note that here C is the capacitance of the insulator only (second layer from bottom in figure 1(a)) and is a constant: $C \neq C(t)$. In our original description of a perovskite RTFS we described the capacitance as illumination-, and hence time-, dependent [3]. However, this present approach for a ZBRS is distinct. Following identical arguments for the charge on the bottom plate, the potential at the top plate is:

$$V_\mathrm{T} = -\frac{Q_\mathrm{B}}{2C}. \tag{6}$$

Taking the first derivative of equation (5) with respect to time yields:

$$\frac{\mathrm{d}V_\mathrm{B}}{\mathrm{d}t} = -\frac{1}{2C}\frac{\mathrm{d}Q_\mathrm{T}}{\mathrm{d}t}. \tag{7}$$

From figure 3, it is clear the current is defined as flowing from the potential at the top plate, V_T, to the potential at the bottom plate, V_B, through the resistor R. This current flow can hence be written using Ohm's Law:

$$I = \frac{V_\mathrm{T} - V_\mathrm{B}}{R}. \tag{8}$$

I can also define the current in terms of the rate of change of charge flowing off the top plate:

$$I = -\left.\frac{\mathrm{d}Q_\mathrm{T}}{\mathrm{d}t}\right|_\mathrm{flow}. \tag{9}$$

The negative sign is present to indicate that if the current is positive (flowing in the direction of the arrow in figure 3), the charge on the top electrode will become less positive over time, as required. Combining equations (7)–(9) yields the expression for change in voltage due to current flow:

$$\left.\frac{\mathrm{d}V_\mathrm{B}}{\mathrm{d}t}\right|_\mathrm{flow} = \frac{1}{2RC}\left(V_\mathrm{T} - V_\mathrm{B}\right). \tag{10}$$

From symmetry I know that $V_\mathrm{T} = -V_\mathrm{B}$, so I can hence say:

$$\left.\frac{\mathrm{d}V_\mathrm{B}}{\mathrm{d}t}\right|_\mathrm{flow} = -\frac{V_\mathrm{B}}{RC}. \tag{11}$$

I can use equation (5) to write this in terms of charge on the top electrode rather than voltage on the bottom:

$$\left.\frac{\mathrm{d}Q_\mathrm{T}}{\mathrm{d}t}\right|_\mathrm{flow} = -\frac{Q_\mathrm{T}}{RC}. \tag{12}$$

The first term on the right-hand side of equation (1) must relate charge generation in the semiconductor to incident optical power density, P. For this simple device model, I will not consider the finite charge generation and recombination times and will instead assume that all charge is generated and recombined instantly. As the absorber is a semiconductor, a conventional power-law relationship between charge and P can be assumed [21]:

$$Q_\mathrm{T,light} = Q_0 P^\gamma. \tag{13}$$

Here Q_0 is a prefactor (which does not have units of C) and γ is a dimensionless exponent that encapsulates the dominant recombination mechanisms in the semiconductor. The first derivative with respect to time is then:

$$\left.\frac{\mathrm{d}Q_\mathrm{T}}{\mathrm{d}t}\right|_\mathrm{light} = Q_0\frac{\mathrm{d}P^\gamma}{\mathrm{d}t}. \quad (14)$$

I have chosen to say that the charge on the top plate will become more positive in response to illumination when Q_0 is positive, but this is arbitrary. In our previous quantitative description of perovskite-based RTFSs, we made the approximation that $\gamma \approx 1/2$ for all materials of interest [11]. This is true only for systems dominated by bimolecular recombination with roughly equivalent populations of electrons and holes [22], and is unlikely to be the case generally. However, we do know that the magnitude of Q_T will increase with P in some form, and this approximation does offer the significant benefit of allowing a single device parameter, with consistent units, to quantify performance. I once again make this assumption but do acknowledge that it is a crude figure of merit, and a non-negligible departure from reality. With this assumption made, the total rate of change of charge density on the top plate can then be defined as:

$$\frac{\mathrm{d}Q_\mathrm{T}}{\mathrm{d}t} = Q_0\frac{\mathrm{d}\sqrt{P}}{\mathrm{d}t} - \frac{Q_\mathrm{T}}{RC}. \quad (15)$$

Using equation (5) to write this in terms of voltages:

$$\frac{\mathrm{d}V_\mathrm{B}}{\mathrm{d}t} = -\frac{Q_0}{2C}\frac{\mathrm{d}\sqrt{P}}{\mathrm{d}t} - \frac{V_\mathrm{B}}{RC}. \quad (16)$$

In this description I am defining the output voltage as the voltage at the bottom plate (as shown in figure 1(c)) and can hence say $V_\mathrm{B} \equiv V_\mathrm{out}$.

$$\frac{\mathrm{d}V_\mathrm{out}}{\mathrm{d}t} = -\frac{Q_0}{2C}\frac{\mathrm{d}\sqrt{P}}{\mathrm{d}t} - \frac{V_\mathrm{out}}{RC}. \quad (17)$$

On inspection, this equation should behave as expected. If $\dot{P} = 0$, then $|V_\mathrm{out}|$ will decay with a time constant defined by $\tau = RC$. Similarly, when $|\dot{P}| > 0$ equation (14) states that V_out can increase or decrease, in competition with decay defined by τ, depending on the sign of Q_0.

Equation (17) was solved numerically using finite difference methods. A square wave of optical power density between 0 and 23.6 mW cm^{-2} with a frequency of 100 Hz was used for the function $P(t)$, as shown in figure 4(a). C was defined using the standard equation for a parallel plate capacitor with d = 300 nm, A = 4 mm^2, and ε_r = 3.9 (for SiO_2). The resistor was set to R = 100 kΩ, as was used for the experimental data shown in figure 2. A value of $Q_0 = 6.5 \times 10^{-14}$ mW$^{-1/2}$ Cm was used as it was found to approximately match experimental observations. The calculated output is shown in figure 4(b). The general form of the output is reproduced accurately: a negative voltage spike in response to the light turning on and a positive spike in response to the light turning off. However, the asymmetry in peak height between the response to the light turning off and the light turning on is not present.

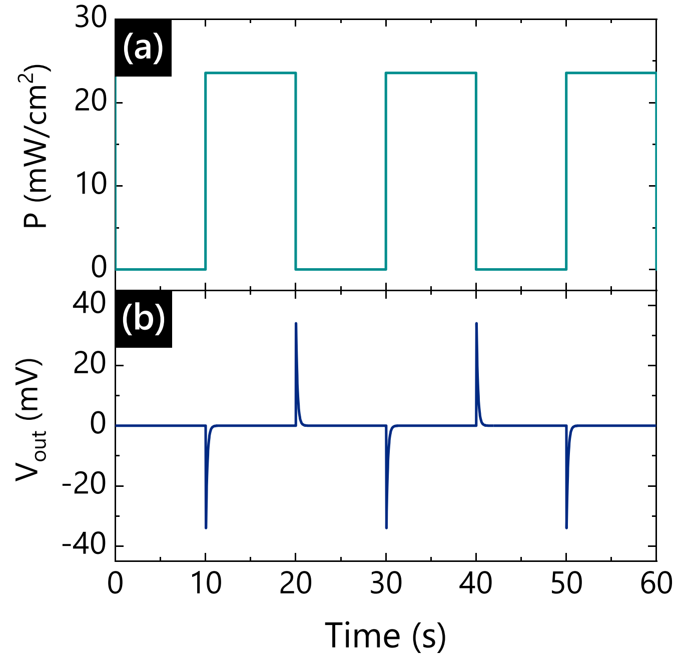

Figure 4. (a) Input optical power density, P, as a function of time used in simple device simulation of ZBRS. (b) Simulated output voltage (V_out) of ZBRS as a function of time calculated using equation (17).

Equation (17) is general and can be used to simulate how a ZBRS responds to an optical power density with any time-dependence, $P(t)$. For this reason, it can also be used to simulate how a 2D array of ZBRSs respond to changes in the visual field, illustrating the potential of these sensors if applied in an 'event camera' [5]. I here followed an analogous approach described in our previous work to demonstrate this [3]. A conventional slow-motion video (recorded at 240 frames per second) was converted to greyscale using the luminosity method. Each pixel in this greyscale video was then converted to an optical power density, P. The output voltage was then calculated as a function of time and position using equation (17). The results are shown in supplementary data video files videos S1 and S2, and some example frames are shown in figure 5. Positive voltages are shown in green, and negative voltages are shown in red. Because the ball is darker than the background, the values of P will be reduced as the ball falls through the frame. For the ZBRSs simulated here, a reduction in intensity is expected to lead to a positive V_out, hence why the ball appears green and the tail appears red.

4.1. Response to a step change in intensity

Equation (17) provides a general relationship between V_out and P, where $P(t)$ can take any form, but in most cases must be solved numerically. However, since the most straight-forward way to characterise a ZBRS is to measure its response to a step function in light intensity, it is worth deriving an analytical expression for this special case.

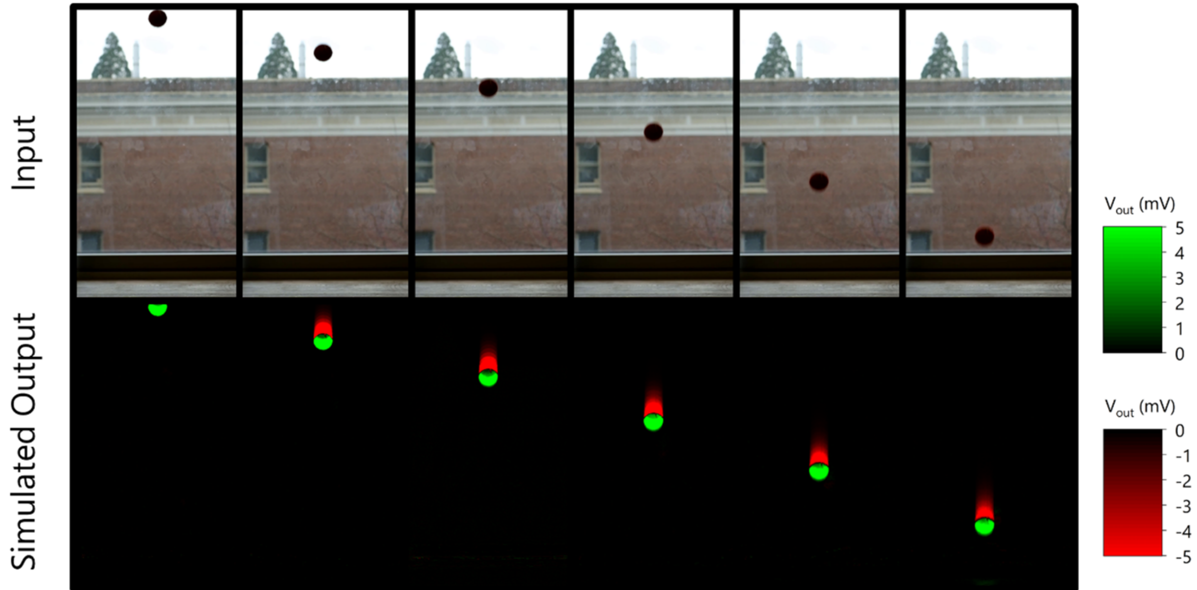

Figure 5. Top: series of input frames of conventional video, recorded at 240 frames per second. Bottom: simulated output of 2D array of ZBRSs exposed to time-dependent optical power density extracted from conventional video shown above. Green signifies a positive output voltage (V_{out}) and red signifies a negative output voltage.

I here follow an analogous, but distinct, approach to that employed in our previous quantitative description of perovskite RTFSs [11]. I start by writing equation (17) as a difference equation by making the following substitutions:

$$\begin{aligned} &\mathrm{d}V_{out} \rightarrow \Delta V_{out} = V_{out,i} - V_{out,i-1} \\ &\mathrm{d}\sqrt{P} \rightarrow \Delta\sqrt{P} = \sqrt{P_i} - \sqrt{P_{i-1}} \\ &V_{out} \rightarrow V_{out,i-1} \\ &\mathrm{d}t \rightarrow \Delta t. \end{aligned} \tag{18}$$

Here $V_{out,i-1}$ is the output voltage immediately before the light intensity was changed, $V_{out,i}$ is the output voltage immediately after the light intensity has been changed, P_{i-1} is the intensity of the light before the step-change and P_i is the intensity of the light after the step change. Δt is the time taken for the light intensity to change from P_{i-1} to P_i, where Δt is normally very small. With these substitutions, the difference equation then reads:

$$V_{out,i} = V_{out,i-1}\left(1 - \frac{\Delta t}{RC}\right) - Q_0\frac{\sqrt{P_i} - \sqrt{P_{i-1}}}{2C}. \tag{19}$$

This expression can be used to quantify the response of a ZBRS when light intensity changes between any two values very rapidly. One value of light intensity does not necessarily need to be zero, nor does the intensity need to be increasing. For the special case of an increase from 0 to P, I define $P_{i-1} = 0$ and $P_i \equiv P$. In this case I assume the ZBRS was in equilibrium before the light was turned on and hence $V_{out,i-1} = 0$. Because $V_{out,i}$ is the voltage immediately after the light is applied, and I am here approximating generation and recombination to be instantaneous, $V_{out,i}$ will be the maximum/minimum voltage of the spike. For this reason, I here re-label $V_{out,i}$ as V_{max}. Even though the subscript is 'max', this value can be positive or negative depending on the sign of Q_0. These conditions lead to the following expression for peak height:

$$V_{max} = -\frac{Q_0\sqrt{P}}{2C}. \tag{20}$$

I can then define a device parameter Λ_0 as follows:

$$\Lambda_0 = -\frac{Q_0}{2C}. \tag{21}$$

The subscript '0' here is to denote zero input voltage, and differentiate it from the figure of merit we previously derived for perovskite RTFSs, which required a finite input voltage [11]. The negative sign is so that a device with a positive Λ_0 will yield a positive voltage spike when light increases. The relationship between V_{max} and P can then be written as follows:

$$V_{max} = \Lambda_0\sqrt{P}. \tag{22}$$

A straight line fit of V_{max} to $\sqrt{P}$ should hence yield Λ_0. It is hoped that this parameter is relatively insensitive to measurement conditions, and can hence serve as a ZBRS figure of merit in an analogous way to power conversion efficiency for solar cells [23] or field effect mobility for thin-film transistors [24]. Λ_0 is a parameter which can be quoted with units of $\mathrm{mW^{-1/2}\,cmV}$, or alternatively $\Omega^{-1/2}\mathrm{m}$ for example. While $\mathrm{mW^{-1/2}\,cmV}$ is a little cumbersome, it is the natural result of using an optical power density in $\mathrm{mW\,cm^{-2}}$ and a voltage in V, and for this reason I will use these units for the remainder of this paper. It is trivial to show that an equivalent expression exists for the response of the device to turning the light off, with the same parameter: Λ_0. Equation (22) states that a

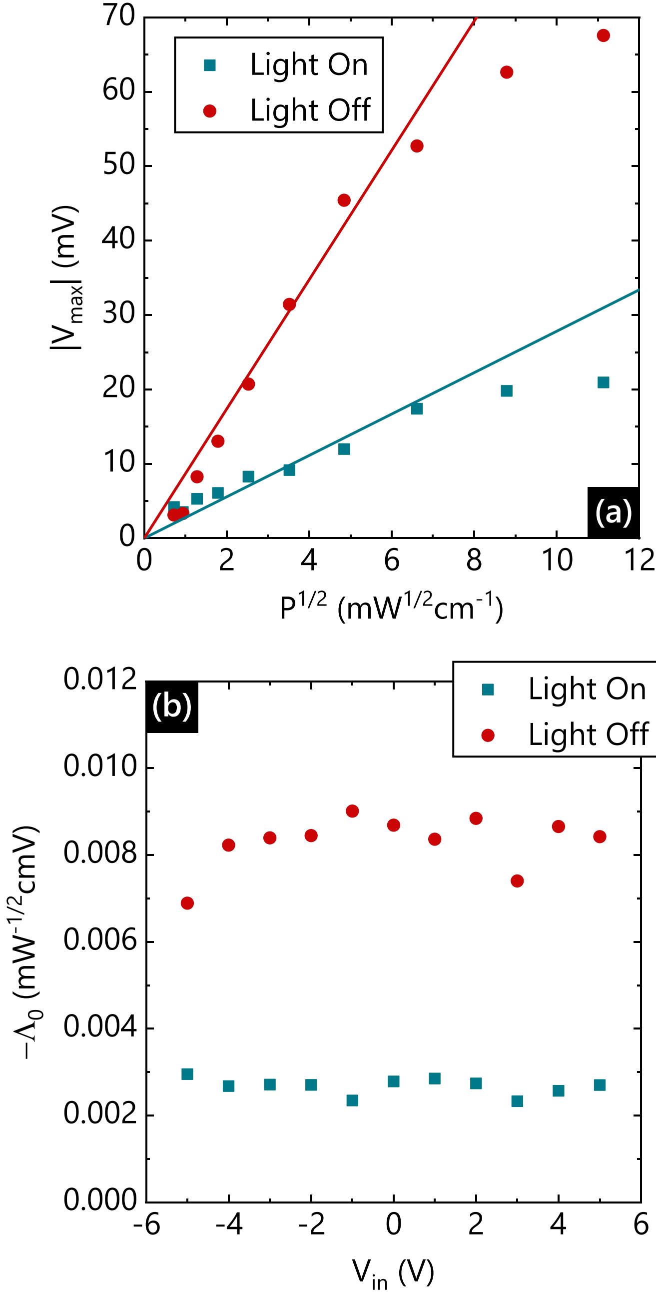

Figure 6. (a) Magnitude of peak value of voltage spike, $V_{\max}$, of ZBRS in response to square wave illumination from 0 to P, as a function of $\sqrt{P}$. Values were extracted from experimental data of V_{out} vs t, in response to light turning on (green) and light turning off (red). (b) Value of ZBRS figure of merit (Λ_0) extracted from experimental $V_{\max}$ vs $\sqrt{P}$ data, using equation (22), as a function of input voltage (V_{in}).

ZBRS with a larger Λ_0, will yield a larger voltage response to changes in light intensity, all else being equal.

An example of experimental $V_{\max}$ plotted as a function of $\sqrt{P}$ for experimental data is shown in figure 6(a). It is clear that $V_{\max}$ does not exhibit a square-root dependence on P, for all values of P. This is not unreasonable as the relative dominance of various recombination mechanisms will depend on the carrier density in the film [25]. For this reason, equation (22) was only fitted to a section of the experimental data: that below 25 mW cm^{-2}. I acknowledge that this distinction is arbitrary, but for the purposes of this report it does allow me to demonstrate a parameterization strategy. The extracted values were $\Lambda_0 = -0.003$ mW$^{-1/2}$ cmV in response to the light turning on, and $\Lambda_0 = -0.008$ mW$^{-1/2}$ cmV in response to the light turning off.

One way to illustrate that these devices are indeed insensitive to input voltage is to measure them as depicted in figure 1(b) with a finite input voltage, V_{in}. Analogous fits to those shown in figure 6(a) were carried out as a function of V_{in}. The results are plotted in figure 6(b), illustrating that V_{in} does not substantially affect this aspect of performance, in this ZBRS design at least.

5. Full treatment of electrons and holes

The strategy described in the previous section enables one to parameterise the performance of a ZBRS, and to consistently quantify differences in behaviour between different devices. However, it clearly makes some substantial simplifications that have the potential to obscure important aspects of the device physics. For example, the approximation of infinite generation and recombination rates results in response with an infinitesimal rise time, which is not observed experimentally. Similarly, it is clear that simply describing charge density in the semiconductor as having a square root dependence on optical power density does not always match experimental observations.

In this section, I provide a more detailed description of the operation of ZBRSs by considering the density of holes and electrons as a function of time and position in the semiconductor. I start with two continuity equations: one for holes and one for electrons:

$$\frac{\partial p(x,t)}{\partial t} = G(x,t) - R_p(x,t) + D_p \frac{\partial^2 p(x,t)}{\partial x^2} \tag{23}$$

$$\frac{\partial n(x,t)}{\partial t} = G(x,t) - R_n(x,t) + D_n \frac{\partial^2 p(x,t)}{\partial x^2}. \tag{24}$$

Here p and n are the three dimensional (3D) concentration of holes and electrons, respectively, x is the distance from the top of the semiconductor, and t is time. The interface between the semiconductor and top electrode is defined as $x = 0$ and the interface between the insulator and semiconductor is defined as $x = L$, where L is the thickness of the semiconductor. $G(x,t)$ is the generation rate, which is the same for holes and electrons (assuming all charge is generated via band-to-band transitions), and $R_p(x,t)$ and $R_n(x,t)$ are the recombination rates for holes and electrons, respectively. The last terms in equations (23) and (24) are diffusion terms, where D_p and D_n are the diffusion coefficients of holes and electrons, respectively.

Because there are no externally applied fields in these devices, and the charges end up being reasonably spatially homogenous after short timescales, I have here neglected drift terms. The generation term describes the number of electrons

or holes per unit volume, generated per second, and is the same for electrons and holes:

$$G(x,t) = \frac{P(t)\lambda\phi e^{-\alpha x}}{hc}\frac{1}{dx}. \quad (25)$$

Here $P(t)$ is the incident optical power density on the device at time t. I have assumed the top electrode is completely optically transparent and hence $P(t)$ is also the incident optical power density at the top of the semiconductor (at $x = 0$). λ is the wavelength of incident photons, ϕ is the charge generation yield, i.e. the number of electrons and holes generated per absorbed photon, and α is the absorption coefficient of the material. h and c are the Planck constant and speed of light *in vacuo*, respectively. The dx term is the infinitesimal distance into the film and is present to ensure the units are correct. $G(x,t)$ is a function describing the 3D generation rate (i.e. with dimensions $\mathrm{L}^{-3}\mathrm{T}^{-1}$), whereas $P(t)$ defines the incident power per unit area.

The recombination rates are defined as follows:

$$R_p(x,t) = k_{1p}p(x,t) + k_2 p(x,t)n(x,t) \quad (26)$$

$$R_n(x,t) = k_{1n}n(x,t) + k_2 p(x,t)n(x,t). \quad (27)$$

Here k_{1p} and k_{1n} are the monomolecular recombination rates for holes and electrons, respectively, k_2 is the bimolecular recombination rate. I have neglected Auger recombination in this formalism because carrier densities are expected to be relatively low under typical operating conditions (say up to $\sim$100 mW cm^{-2}). For the purposes of this study, I have approximated $k_{1p} = k_{1n}$ in all cases. While it is unlikely that the nature of trapping will be identical for electrons and holes, especially at the bare SiO_2 interface [26], this condition is enforced to illustrate how asymmetry in the properties of the metal/semiconductor interface alone can lead to the observed behaviour.

Including generation and recombination terms, equations (23) and (24) can then be written as:

$$\frac{\partial p(x,t)}{\partial t} = \frac{P(t)\lambda\phi e^{-\alpha x}}{hc}\frac{1}{dx} - k_{1p}p(x,t) - k_2 p(x,t)n(x,t) + D_p\frac{\partial^2 p(x,t)}{\partial x^2} \quad (28)$$

$$\frac{\partial n(x,t)}{\partial t} = \frac{P(t)\lambda\phi e^{-\alpha x}}{hc}\frac{1}{dx} - k_{1n}n(x,t) - k_2 p(x,t)n(x,t) + D_n\frac{\partial^2 p(x,t)}{\partial x^2}. \quad (29)$$

Equations (28) and (29) are coupled non-linear 2nd order partial differential equations and must be solved numerically. The approach I use here to evaluate $p(x,t)$ and $n(x,t)$ is analogous to past approaches [27], and employs finite difference methods. Four boundary conditions employed are listed in equation (30)–(33). They state that no charge can exit the bottom of the semiconductor (through the insulator) and that at time $t = 0$ the semiconductor is absent of any charge:

$$\frac{\partial(L,t)}{\partial t} = 0 \quad (30)$$

$$\frac{\partial n(L,t)}{\partial t} = 0 \quad (31)$$

$$p(x,0) = 0 \quad (32)$$

$$n(x,0) = 0. \quad (33)$$

To incorporate the effect of holes being able to leave the semiconductor through the top electrode, but electrons not being able to, I also define the following two further conditions. The first, forbidding electrons exiting through the top contact, is given by equation (34):

$$\frac{\partial n(0,t)}{\partial t} = 0. \quad (34)$$

The other condition is that for every time step in the calculation, the concentration of holes at the first position step ($x = 0$) will be reduced by some amount, S, encapsulating holes leaving the system through the top electrode. Because equations (28) and (29) will be solved using a finite difference technique, the rate at which holes are removed using this strategy will depend on the choice of time and space steps. For this reason, the parameter S is not comparable between calculations, and will here be adjusted to roughly match experimental results. In the absence of a detailed electronic description of the interface, this is a relatively simple way to encapsulate the asymmetry of holes and electrons at the interface.

Figure 7 shows the density of holes and electrons calculated as a function of depth into the semiconductor using equations (28) and (29), under constant illumination. The parameters employed in this simulation are provided in table 1. Figure 7(a) shows the concentration profile after 1 ps, figure 7(b) shows the concentration profile after 1 ns, figure 7(c) shows the concentration profile after 1 μs. Figure 7 illustrates that at short timescales the concentration of holes and electrons are comparable, and it is not until the time passed is on the same order of magnitude as the monomolecular recombination lifetimes that an appreciable difference occurs.

Under steady state conditions the relative concentration of holes and electrons is anticipated to depend on the value of S. Figure 8 shows the mean density of holes and electrons throughout the film calculated as a function of time under constant illumination at $P = 100$ mW cm^{-2} for 1 μs, followed by being held in the dark ($P = 0$ mW cm^{-2}) for a further 1 μs, for several values of S. All other parameters were kept constant for all calculations. In all cases an equilibrium is observed after a few 100's of nanoseconds.

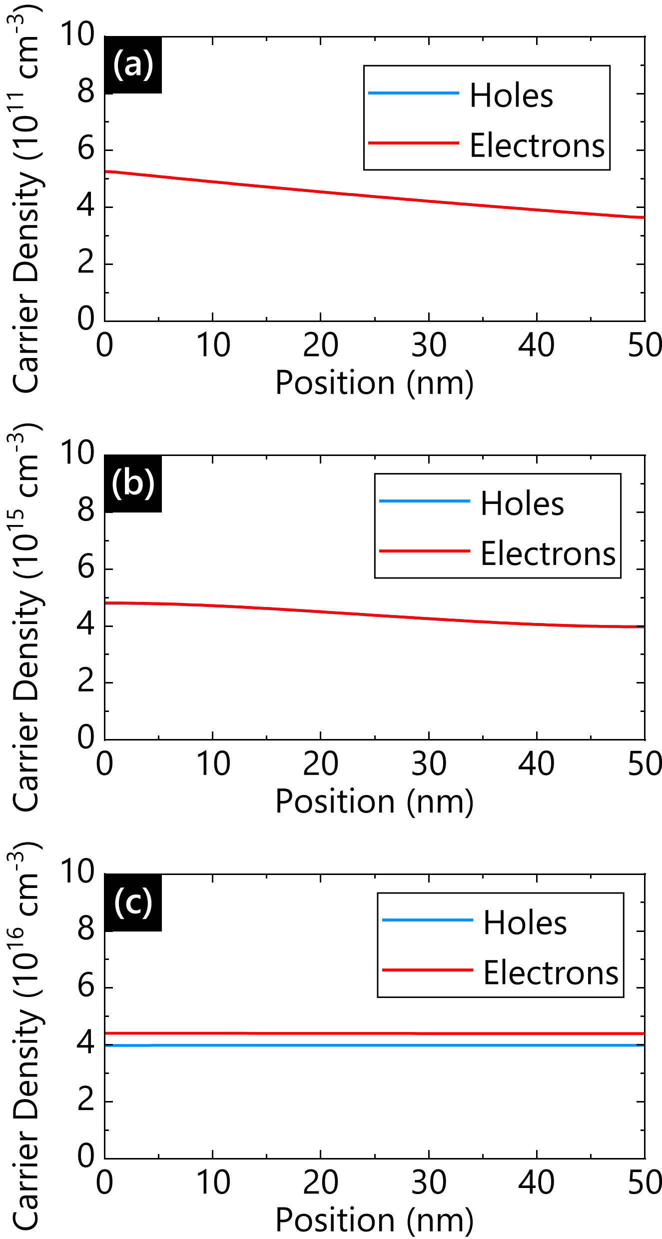

Figure 7. Three-dimensional density of holes (blue) and electrons (red) as a function of distance from the top of the semiconductor film, calculated using equations (28) and (29) and the values listed in table 1, after (a) 10^{-12} s, (b) 10^{-9} s, and (c) 10^{-6} s constant illumination at $P = 10$ mW cm^{-2}.

With monomolecular lifetimes on the order of 100 ns, the data in figure 8 suggests steady state conditions can be approximated from data obtained after 1 μs. Figure 9 shows the average concentration of holes and electrons, and their difference, throughout the film after 1 μs of constant illumination, as a function of S.

As expected, as the metal/semiconductor interface becomes more efficient at extracting holes (higher S), the number of holes in the film under steady state conditions drops, and the net charge increases. To relate $p(x,t)$ and $n(x,t)$ to device

Table 1. List of parameters used in the simulations in section 5, with rationale for choice of value.

Parameter	Value	Rationale
$P(t)$	10 mW cm^{-2}	Constant illumination at ~outdoor intensity.
λ	535 nm	Peak emission intensity of experimental illumination source.
ϕ	1	All absorbed photons assumed to result in free charges (for simplicity).
α	7.5×10^6 m^{-1}	Approximated from optical measurements.
k_{1p}	1×10^7 s^{-1}	Order of magnitude of monomolecular recombination in P3HT:PCBM [28].
k_{1n}	1×10^7 s^{-1}	Order of magnitude of monomolecular recombination in P3HT:PCBM [28].
k_2	2×10^{-13} cm^3 s^{-1}	Approximate value of bimolecular recombination in P3HT:PCBM [29].
D_p	3×10^{-7} m^2 s^{-1}	Set assuming a mobility of 0.1 cm^2 V^{-1} s^{-1}, [30] and temperature of 300 K.
D_n	3×10^{-7} m^2 s^{-1}	Set assuming a mobility of 0.1 cm^2 V^{-1} s^{-1}, [31] and temperature of 300 K.
S	1×10^{-4}	
Δt	2×10^{-13} s	Chosen time step
Δx	5×10^{-10} m	Chosen spatial step size
L	50 nm	Typical film thickness.

parameters, I sum the charge in the semiconductor and identify this as the charge on the top plate of the capacitor:

$$Q_{\mathrm{T}}(t) = eA \int_L^0 [p(x,t) - n(x,t)]\,\mathrm{d}x. \tag{35}$$

Here, e is the magnitude of the charge on an electron and A is the ZBRS lateral area. This $Q_{\mathrm{T}}(t)$ can then be used instead of the $Q_T(t)$ in equation (12). i.e. there is no longer an explicit square-root-dependence on P. To evaluate device parameters, an analogous procedure is followed: at each time-step in the finite difference calculator $Q_T(t)$ is calculated using equation (35), this is then used to update $V_{\mathrm{out}}(t)$ from the circuit parameters. Figure 10(a) shows a square wave of $P(t)$ as a function of time, and figure 10(b) shows $V_{\mathrm{out}}(t)$ calculated as a function of time in response to this optical stimulus for $S = 10^{-4}$ and three different values of R.

The spiking device behaviour is reproduced, with a higher resistance leading to a longer decay as expected. While a finite rise time is now present in this data, this model is still not able to reproduce the asymmetry between the light turning on and turning off observed experimentally. This remains an

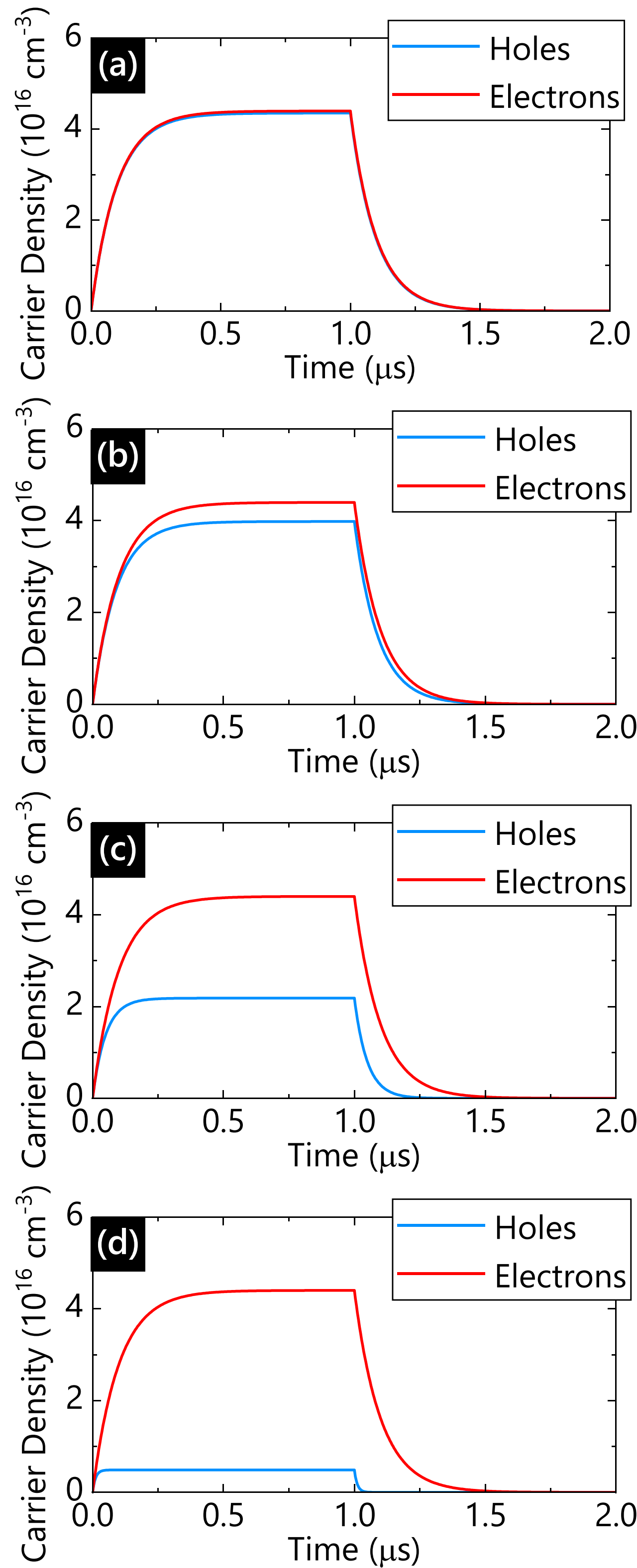

Figure 8. Calculated average three-dimensional density of holes (blue) and electrons (red) throughout the semiconductor film, as a function of time under illumination (first 1 μs) and in the dark (last 1 μs), calculated using equations (28) and (29) and the values listed in table 1, but with a value of $S =$ (a) 10^{-5}, (b) 10^{-4}, (c) 10^{-3}, (d) 10^{-2}.

unanswered question in the behaviour of ZBRSs, and a target for future studies. However it is likely to be a result of the asymmetry of the semiconductor:electrode interface to holes and electrons. The timescales considered in figure 10(b) are roughly three orders of magnitude longer than those in figure 8. It is important to note that a steady-state charge density is still

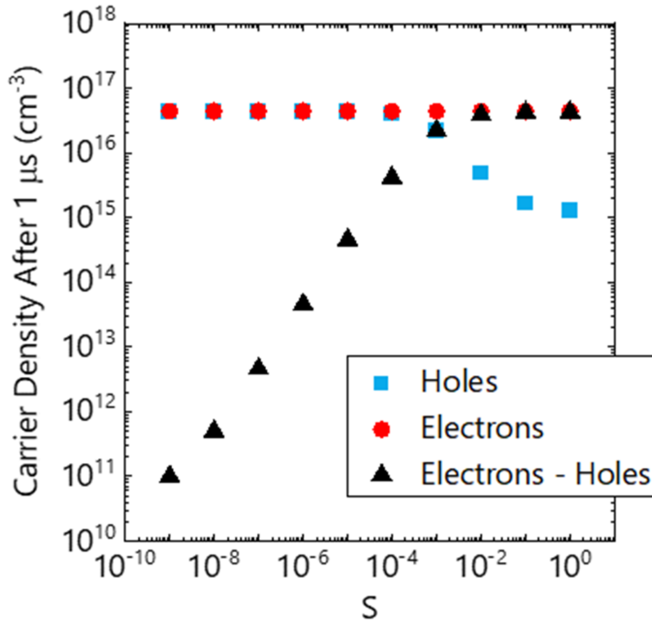

Figure 9. Calculated average 3D density of holes (blue squares), electrons (red circles), and their difference (black triangles), throughout semiconductor film, after 1 μs constant illumination at 100 mW cm^{-2}, as a function of S.

established over timescales $\sim$1 μs, but the device response in figure 10(b) is now dominated by the RC time constant of the device. This result implies that as long as the decay occurs over timescales of $\gtrsim$1 μs, one should still be able to tune the decay through a choice of external resistor for this semiconductor system.

Figure 10(c) shows the device lifetime (τ), extracted assuming a monoexponential decay, as a function of R. As expected, the device lifetime decreases exponentially as R is decreased, down to around 100 ns with the parameters chosen in table 1. Below this value, τ is expected to be limited by the recombination rates in the semiconductor: k_{1p}, k_{1n}, and k_2. When a device response faster than say 1 μs is required, one could use a material with a faster monomolecular decay rate, at the expense of peak height. This then leads to the counterintuitive conclusion that semiconductors with more traps could give rise to better device performance (from a response-time point of view at least).

Figure 10(c) also shows the magnitude of the peak voltage signal, $|V_{\mathrm{max}}|$, calculated as a function of resistance. Significantly, the magnitude of the maximum voltage is observed to increase as the resistance is increased. We observed this behaviour experimentally in our previous report [10] but attributed it to the existence of a finite contact resistance between the semiconductor and top electrode. However, since contact resistance is not part of this present model, it cannot alone be responsible for the behaviour observed. It is more likely that the voltage-dependence is simply the result of the fact the output parameter is a voltage, and the number of charges generated is insensitive to the resistance. Ohm's Law tells us that for a given current, the voltage will increase with resistance.

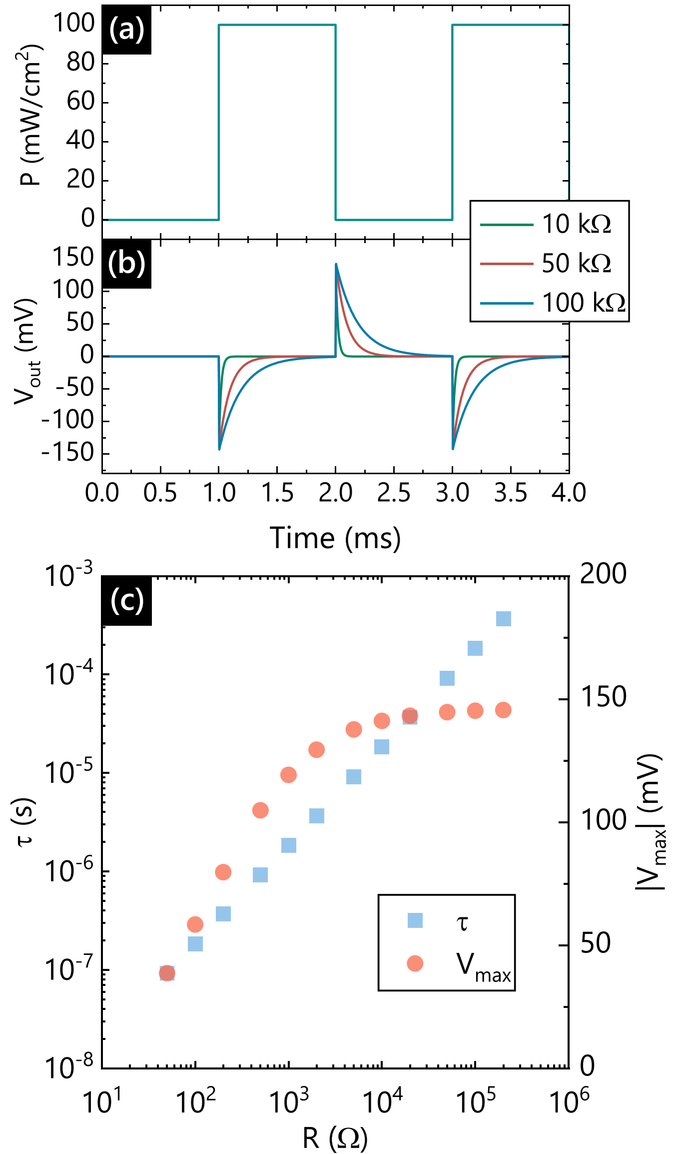

Figure 10. (a) Simulated input optical power density, P, as a function of time applied to ZBRS. (b) Simulated output voltage, V_{out}, of ZBRS as a function of time calculated using equations (12) and (34). All parameters were as listed in table 1, with the exception of resistance, R, which was varied as described in the figure legend. (c) Decay constant, τ, and magnitude of maximum voltage, $|V_{\mathrm{max}}|$, of ZBRS after application of step-function in optical power density, as a function of R, evaluated assuming a monoexponential decay.

6. Conclusions

I have presented a mathematical framework to quantify and predict the behaviour of ZBRSs. By describing the charge on the two plates of the capacitor separately, where the charge on the top plate is determined by the properties of the semiconductor and illumination conditions, a simple device model has been derived relating the output voltage to incident optical power density. A more detailed model was also derived in which the relative densities of holes and electrons were evaluated directly, yielding equivalent behaviour to the simple

device model. A ZBRS figure of merit, Λ_0, was identified which is hoped to enable facile comparison of devices between different research groups.

This work represents a necessary step to understand and parameterise ZBRSs. There still remains work to be done on a complete theoretical description of these devices, in particular a way to encapsulate the asymmetry between the spike height when the light is turned on compared to when it is turned off. Nonetheless, this framework provides a thorough and consistent description of these devices, provides a clear means to evaluate performance limits, and a way to develop strategies to improve practical functionality in the future.

Data availability statement

The data that support the findings of this study are available upon reasonable request from the authors.

Acknowledgments

The author thanks the National Science Foundation for financial support (Award No. 1942558). Part of this research was conducted at the Northwest Nanotechnology Infrastructure, a National Nanotechnology Coordinated Infrastructure site at Oregon State University which is supported in part by the National Science Foundation (Grant NNCI-2025489) and Oregon State University.

ORCID iD

John G Labram https://orcid.org/0000-0001-6562-9895

References

[1] Adrian E D and Matthews R 1927 The action of light on the eye *J. Physiol.* **64** 279–301

[2] Hartline H K and Graham C H 1932 Nerve impulses from single receptors in the eye *J. Cell. Comp. Physiol.* **1** 277–95

[3] Trujillo Herrera C and Labram J G 2020 A perovskite retinomorphic sensor *Appl. Phys. Lett.* **117** 233501

[4] Posch C, Serrano-Gotarredona T, Linares-Barranco B and Delbruck T 2014 Retinomorphic event-based vision sensors: bioinspired cameras with spiking output *Proc. IEEE* **102** 1470–84

[5] Gallego G *et al* 2022 Event-based vision: a survey *IEEE Trans. Pattern Anal. Mach. Intell.* **44** 154–80

[6] Mead C A and Mahowald M A 1988 A silicon model of early visual processing *Neural Netw.* **1** 91–97

[7] Delbrück T and Mead C A 1989 An electronic photoreceptor sensitive to small changes in intensity *Advances in Neural Information Processing Systems* vol 1 pp 720–7

[8] Snaith H J 2018 Present status and future prospects of perovskite photovoltaics *Nat. Mater.* **17** 372–6

[9] Wadsworth A, Hamid Z, Kosco J, Gasparini N and McCulloch I 2020 The bulk heterojunction in organic photovoltaic, photodetector, and photocatalytic applications *Adv. Mater.* **32** 2001763

[10] Trujillo Herrera C and Labram J G 2021 An organic retinomorphic sensor *ACS Appl. Electron. Mater.* **4** 92–98

[11] Herrera C T and Labram J G 2021 Quantifying the performance of perovskite retinomorphic sensors *J. Phys. D: Appl. Phys.* **54** 475110

[12] Hu L, Noda Y, Ito H, Kishida H, Nakamura A and Awaga K 2010 Optoelectronic conversion by polarization current, triggered by space charges at organic-based interfaces *Appl. Phys. Lett.* **96** 243303

[13] Tomimatsu A, Yokokura S, Reissig L, Dalgleish S, Matsushita M M and Awaga K 2019 Rate-determining process in MISIM photocells for optoelectronic conversion using photo-induced pure polarization current without carrier transfer across interfaces *Phys. Chem. Chem. Phys.* **21** 13440–5

[14] Reissig L, Mori K, Treadwell R, Dalgleish S and Awaga K 2016 Factors affecting the polarity and magnitude of photoresponse of transient photodetectors *Phys. Chem. Chem. Phys.* **18** 6821–30

[15] Reissig L, Dalgleish S and Awaga K 2016 A differential photodetector: detecting light modulations using transient photocurrents *AIP Adv.* **6** 015306

[16] Zhang X and Labram J 2022 Role of blend ratio in bulk heterojunction organic retinomorphic sensors *J. Mater. Chem.* C **10** 12998–3004

[17] Irwin M D, Buchholz D B, Hains A W, Chang R P H and Marks T J 2008 p-Type semiconducting nickel oxide as an efficiency-enhancing anode interfacial layer in polymer bulk-heterojunction solar cells *Proc. Natl Acad. Sci.* **105** 2783–7

[18] Clarke T M and Durrant J R 2010 Charge photogeneration in organic solar cells *Chem. Rev.* **110** 6736–67

[19] Feynman R P, Leighton R B and Sands M 2015 *The Feynman Lectures on Physics, Vol. II: The New Millennium Edition: Mainly Electromagnetism and Matter* (New York: Basic Books)

[20] Chattopadhyay S and Labram J G 2021 The effect of substrate curvature on capacitance and current–voltage characteristics in thin-film transistors on flexible substrates *J. Phys. Mater.* **4** 025002

[21] Levine I, Gupta S, Brenner T M, Azulay D, Millo O, Hodes G, Cahen D and Balberg I 2016 Mobility–lifetime products in $MAPbI_3$ films *J. Phys. Chem. Lett.* **7** 5219–26

[22] Balberg I 1994 The two carriers' mobility-lifetime products and their light intensity dependencies in hydrogenated amorphous silicon *J. Appl. Phys.* **75** 914–23

[23] Green M A, Dunlop E D, Hohl-Ebinger J, Yoshita M, Kopidakis N and Hao X 2021 Solar cell efficiency tables (version 58) *Prog. Photovolt. Res. Appl.* **29** 657–67

[24] Paterson A F, Singh S, Fallon K J, Hodsden T, Han Y, Schroeder B C, Bronstein H, Heeney M, McCulloch I and Anthopoulos T D 2018 Recent progress in high-mobility organic transistors: a reality check *Adv. Mater.* **30** 1801079

[25] Herz L M 2016 Charge-carrier dynamics in organic-inorganic metal halide perovskites *Annu. Rev. Phys. Chem.* **67** 65–89

[26] Chua L-L, Zaumseil J, Chang J-F, Ou E C-W, Ho P K-H, Sirringhaus H and Friend R H 2005 General observation of n-type field-effect behaviour in organic semiconductors *Nature* **434** 194–9

[27] Watts C L, Aspitarte L, Lin Y-H, Li W, Elzein R, Addou R, Hong M J, Herman G S, Snaith H J and Labram J G 2020 Light soaking in metal halide perovskites studied via steady-state microwave conductivity *Commun. Phys.* **3** 1–10

[28] Ferguson A J, Kopidakis N, Shaheen S E and Rumbles G 2011 Dark carriers, trapping, and activation control of carrier recombination in neat P3HT and P3HT:PCBM blends *J. Phys. Chem.* C **115** 23134–48
[29] Kniepert J, Schubert M, Blakesley J C and Neher D 2011 Photogeneration and recombination in P3HT/PCBM solar cells probed by time-delayed collection field experiments *J. Phys. Chem. Lett.* **2** 700–5
[30] Sirringhaus H *et al* 1999 Two-dimensional charge transport in self-organized, high-mobility conjugated polymers *Nature* **401** 685–8
[31] Wöbkenberg P H, Bradley D D C, Kronholm D, Hummelen J C, de Leeuw D M, Cölle M and Anthopoulos T D 2008 High mobility n-channel organic field-effect transistors based on soluble C_{60} and C_{70} fullerene derivatives *Synth. Met.* **158** 468–72